ISBN: 978-3-95450-232-5 ISSN: 2673-7000 doi:10.18429/JACoW-NAPAC2022-WEPA08

DESIGN AND OPERATION EXPERIENCE OF A MULTI-COLLIMATOR/YAG SCREEN DEVICE ON LCLS II LOW ENERGY BEAMLINE*

X. Liu†, C. Adolphsen, M. Santana-Leitner, L. Xiao, F. Zhou
SLAC National Accelerator Laboratory, Menlo Park, CA, USA

Abstract

A new device has been designed and installed on the Linac Coherent Light Source II (LCLS II) injector low energy beamline. It is made of a 15 mm copper plate, with four round apertures of 6, 8, 10, and 12 mm radius respectively. Two yttrium aluminum garnet (YAG) screens and their corresponding mirrors are added at the end of the collimator plate for beam/halo profile imaging. The collimator plate is electrically insulated from the chamber so that it can also be used for measuring the dark current. A motor-driven ultrahigh vacuum (UHV) compatible linear translator shifts the device between positions. Besides design details, beam dynamics and radiation analyses as well as operation experience are presented.

INTRODUCTION

In advance of the installation of LCLS II main linac, commissioning of its normal conducting Very High Frequency (VHF) radio frequency (RF) gun started a few years ago with the low energy beamline. It was observed that field emission (dark current) of roughly 2 μA level was present under normal operation of the gun. While the dark current of this level is deemed manageable with existing beamline configurations, it is desired in precaution to add a collimator on the low energy beamline to block the dark current, in case that the dark current situation worsens over time. It is desired to have multiple aperture sizes due to the unpredictability of possible new field emitters. YAG screens are also required on the same device for beam and halo profile monitoring. In addition, it is desired for the device to have the capability to measure dark current.

MECHANICAL DESIGN

Since the device has 7 different nominal operating positions, it utilizes a motorized UHV compatible linear translator to change position instead of an air cylinder, which is commonly used in a typical in-and-out actuation. See Figure 1 for the 3D model of the assembly. A translation degree of freedom in the other transverse (x) direction is also desired for precision positioning of the collimator, but it is impractical because of space constraints. The alignment error in x direction is controlled to within acceptable range by using special assembly features and machining sequences.

Figure 2 shows the collimator plate subassembly. Both the collimator plate and the shaft are made of oxygen-free electronic (OFE) copper. The thickness of the collimator is chosen based on radiation simulation. The large cross section area ensures effective conduction of heat from the collimator plate to outside of the collimator flange. The radius of the four circular apertures are 6, 8, 10, and 12 mm respectively. The spacing between the collimator apertures is made large enough so that the aperture is the only direct pass through the device when the center of the aperture is aligned with the axis of the beam pipe.

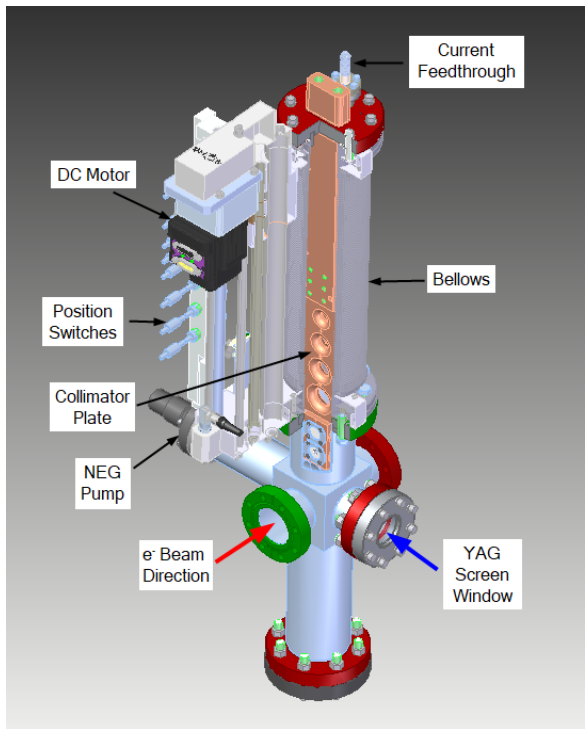

Figure 1: A cut-away view of the 3D model of the device. The absolute linear encoder and the radiation shielding enclosure are not shown in this view.

The YAG screens have a diameter of 20 mm and a thickness of 50 μm. They have a 20-nm-thick indium tin oxide (ITO) coating on one side to prevent accumulating charges. They are clamped securely in place with an annealed copper wire around the edge to ensure reliable electrical contact and mechanical support. The 45° mirrors are made of 304L stainless steel and polished to mirror finish. The thickness of the mirrors is 1 mm.

On the air side of the triaxial current feedthrough, a bleeding resistor connects the collimator plate to the chamber ground to prevent the collimator from becoming electrically floating when the current signal cable is disconnected.

* Work supported by US DOE under contract AC02-76SF00515.
† liuxh@slac.stanford.edu

ISBN: 978-3-95450-232-5 ISSN: 2673-7000 doi:10.18429/JACoW-NAPAC2022-WEPA08

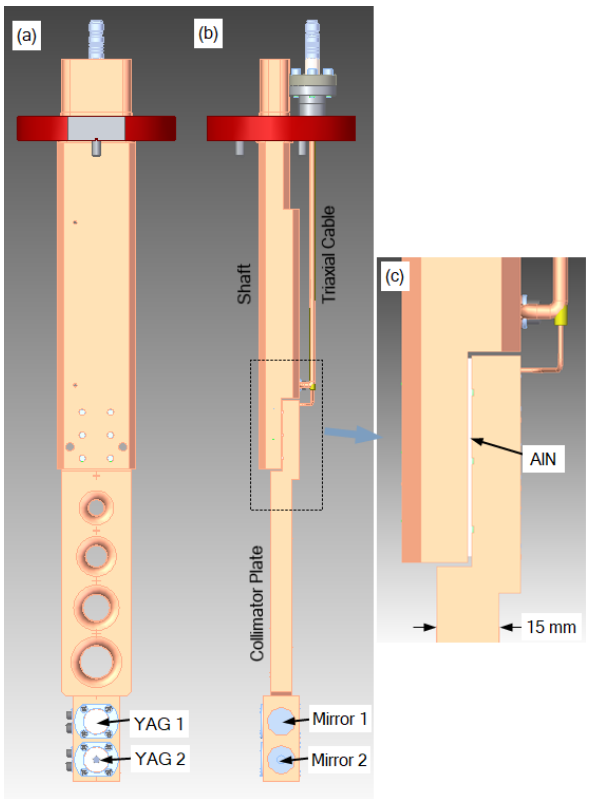

Figure 2: Front (a) and side (b) views of the collimate plate subassembly. The aperture sizes from top to bottom are 6, 8, 10, and 12 mm in radius respectively. The edges of the apertures are rounded to 6.5 mm radius on both sides. A 1 mm thick AlN spacer (c) insulates the collimator plate electrically. 6 screws connect the collimator plate to the shaft, providing good thermal contact.

WAKEFIELD SIMULATIONS

When an electron beam passes through the collimator, it can generate wakefields inside. SLAC-developed parallel finite-element electromagnetic code suite ACE3P is used to simulate the collimator wakefields and evaluate their effects to the beams [1].

Simulation Models

The collimator can work at various nominal positions during LCLS II operation. In this section we present the wakefield simulation results for three cases: the fully extracted collimator, the collimator inserted with 12 and 4 mm radius apertures respectively. Since the mechanical parts behind the collimator plate are far away from the beams, they are not included in the simulation models. It should be noted that the simulation models in this section, as shown in Figure 3, are based on the preliminary design, which has circular apertures of 2, 4, 8, and 12 mm radius instead. However, the simulation results are still relevant in validating the collimator design.

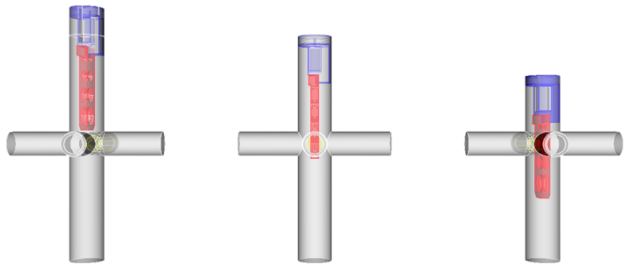

Figure 3: Collimator wakefield simulation models. Collimator fully extracted (left), collimator inserted with 12 mm (middle) and 4 mm (right) radius apertures.

Short Range Wakefields

The beam length of 2.5 mm is assumed for LCLS II. The short range longitudinal and transverse wakefields are carried out using ACE3P time domain code T3P. The summary results of the loss and kicker factors in the three cases are listed in Table 1. The collimator wakefield profiles at the worst case are shown in Figure 4.

Table 1: Wakefield Results for Bunch Length of 2.5 mm

Collimator Position	Loss Factor [V/pC]	Kick Factor_x [V/pC/mm]	Kick Factor_y [V/pC/mm]
4 mm	5.26	0.5	0.5
12 mm	2.58	$4.5 \cdot 10^{-2}$	$4.7 \cdot 10^{-2}$
Fully Extracted	0.93	9.8·10-3	1.2·10-2

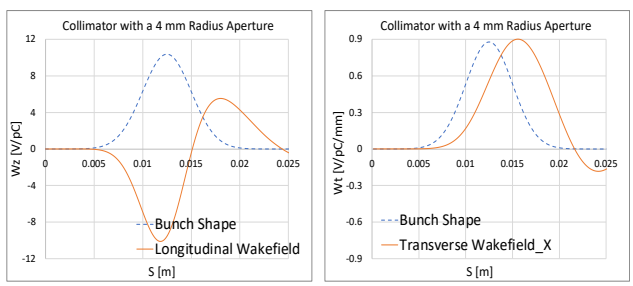

Figure 4: The collimator longitudinal (left) and transverse at x-direction (right) wakefields at the worst scenario.

For 100 pC per bunch charge, 0.1 mA current in LCLS II, the total beam power loss in the collimator is no more than 53 mW due to the longitudinal wakefield. The beam emittance growth due to the transverse wakefield is ~ 1%.

Trapped Modes

The longitudinal HOM spectrum in the collimator with a 4 mm radius aperture from T3P is shown in Figure 5. The most dangerous trapped mode is around 2.4 GHz. Then ACE3P eigensolver Omega3P is used to search for this mode and the simulation shows that if the mode hits the beam spectrum, the resonant power loss is less than 0.3 mW, which is not of concern.

ISBN: 978-3-95450-232-5 ISSN: 2673-7000 doi:10.18429/JACoW-NAPAC2022-WEPA08

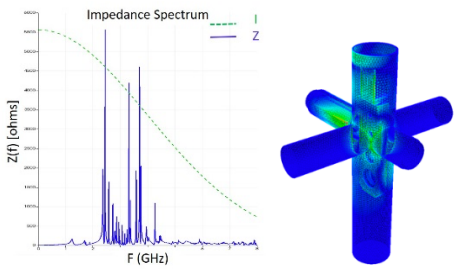

Figure 5: The HOM impedance spectrum in the collimator (left) and the trapped mode around 2.4 GHz (right).

RADIATION TRANSPORT CALCULATIONS

Radiation transport calculations were carried out in order to validate the efficacy of the new collimator in suppressing dark current propagation and limiting irradiation of sensitive components in the vicinity of the collimator.

In a FLUKA [2, 3] model of the injector with a detailed implementation of all the apertures from the gun to the first cryomodule shown in Figure 6 and using a source routine that emulates the observed dark current distribution hitting an 8-20 mm ID tapered copper collimator of up to 15 mm thickness, only *one* electron was found to reach the first cryomodule for each 10 million dark current electrons, accompanied by a few photons carrying a total of 1 eV (of 750 keV). Moreover, the likelihood of enhanced dark current production from backscattered radiation to the gun was deemed low, as just about 7 photons per million dark current electrons on the collimator would reach back to the gun, with an average energy of 10 eV.

Simulations also suggested that the collimator could cut down by over two orders of magnitude to ~3 rad/h the irradiation of the Vitton seals of a valve placed 35 cm downbeam of the collimator. As for backscattered current through the laser windows placed at a similar distance upbeam of the collimator, the found value was well below half a nanoamp.

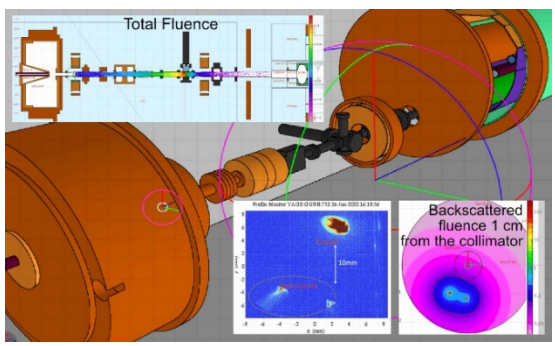

Figure 6: Rendering Ref. [4] of the FLUKA geometry used for radiation transport simulations in the injector along with screenshots of the measured dark current at the YAG screen, the fluence [cm^2/e^-] of simulated dark current onto the collimator and the backscattered radiation 1 cm upbeam of it, and the total fluence propagation.

BEAM OPERATION EXPERIENCES

The collimator/YAG screen device has been installed and operated during LCLS II injector commissioning. The collimating function works well with the 12 mm radius aperture sufficient to block majority of the dark current while posing negligible impact to beam performance. Figure 7 shows an example of the correlation between the measured dark current and the collimator size. The YAG screens with conductive coating have completely eliminated the intermittent discharge phenomenon, which was observed on previous uncoated YAG screens. The current measurement capability of the collimator plate turns out to be a valuable bonus from the device, making it possible to have a convenient and reliable monitor of the dark current status.

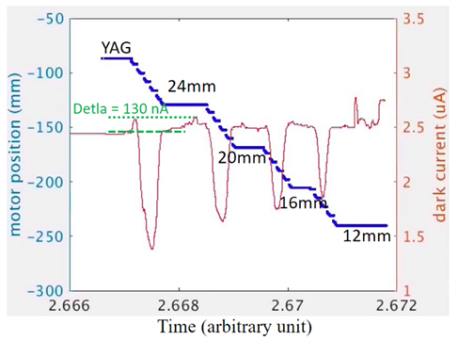

Figure 7: Dark current (red) intercepted by the collimator correlated with collimator position (blue). The corresponding aperture size at each static position is also labeled. It indicates that roughly 95% of the dark current is blocked even with the 24 mm collimating aperture.

ACKNOWLEDGEMENTS

We would like to thank Dr. Jeremy Mock, Dr. Alex Montironi, Ms. Namrata Balakrishnan, and Dr. Bryce Jacobson for their help on electronics and motion control, and Dr. Yuantao Ding for providing Figure 7. The research used resources of the National Energy Research Scientific Computing (NERSC) Center, which is supported by the Office of Science of the U.S. Department of Energy under Contract No. DE-AC02-05CH11231.

REFERENCES

[1] L. Xiao, L. Ge, Z. Li, and C.-K. Ng, "Advances in Multiphysics Modelling for Parallel Finite-Element Code Suite ACE3P", *IEEE J. Multiscale Multiphysics Comput. Tech.*, vol. 4, pp. 298–306, 2019. doi:10.1109/JMMCT.2019.2954946

[2] T. T. Bohlen *et al.*, "The FLUKA Code: Developments and Challenges for High Energy and Medical Applications", *Nucl. Data Sheets*, vol. 120, pp. 211–214, 2014. doi:10.1016/j.nds.2014.07.049

[3] A. Ferrari, P. R. Sala, A. Fasso, and J. Ranft, "FLUKA: a multi-particle transport code", CERN-2005-10, 2005. doi:10.2172/877507

[4] V. Vlachoudis, "FLAIR: A Powerful but User Friendly Graphical Interface For FLUKA", in *Proc. M&C'09*, Saratoga Springs, NY, USA, May 2009, pp. 790–800.